9 SCIENTIFIC HIGHLIGHT OF THE MONTH

Full-Potential Local-Orbital Minimum-Basis Scheme

FPLO

Klaus Koepernik, Helmut Eschrig, Ingo Opahle, Ulrike Nitzsche, Igor Chaplygin,
and Manuel Richter

*Department of Theoretical Solid State Physics, Leibniz-Institut für Festkörper- und
Werkstoffforschung Dresden e.V., P.O. box 270 116, D-01171 Dresden, Germany*

Introduction

Every chapter of the well-known textbook *Principles of the Theory of Solids* by J.M. Ziman is headed by a particular quotation. For example, the chapter about *Electronic states* is introduced by R. Kipling's words

**There are nine and sixty ways of constructing tribal lays,
And-every-single-one-of-them-is-right.**

What Kipling wrote is certainly true. (Who would ever doubt this ?) Also, Ziman took a good choice of the heading, since he intended to emphasize the equivalence of band structure methods **in principle**. Everybody who has been working in our field of electronic structure theory knows, however, that **quantitative** comparisons between recent codes, on a physically relevant scale of accuracy, are still unsatisfactory. This statment does not refer to the never ending discussion if LSDA, GGA, LDA+U, or SIC-LSDA is the preferrable approximation to density functional theory for a given system. What is meant is the purely numerical implementation of a well-defined task. Take six different band structure codes and let them calculate the lattice constant of fcc thorium in LDA. You will get five answers deviating from each other by much more than related experimental data, see Figure 9 in Section . Remember, we do not want to discuss the well-known problem of overbinding in LDA ! *This problem can only be tackled if we know what the LDA result is.*

At this point it is fair to state that tremendous advances in the numerical techniques have been achieved since John Slater's days. A number of full-potential methods with a high degree of reliability and flexibility have been developed.[1] The price that has to be paid for the accuracy consists of computing time and main storage: linear methods require large basis sets, while non-linear schemes are slow anyway.

Despite the worldwide efforts spent in developing accurate electronic structure code, we are not aware of any reasonable data collection, except that discussed below, comparing the key quantity of DFT, the ground state energy, obtained with essentially different schemes. There is a wide-spread opinion that the numerical accuracy of the codes is more or less unknown. However, if the total energies produced by completely independent codes with tenthousands of command lines would almost coincide, the probability that the codes have noticable errors would be accordingly small.

This highlight is devoted to a recently developed code that provides answeres to both questions raised. The full-potential local-orbital minimum-basis (FPLO) code [1] is

(i) numerically (almost) as efficient as wide-spread lower-accuracy schemes. This efficiency is based on employing a self-adjusting minimum basis. The valence basis is completed by a few upper core states and polarization states.

(ii) The total energy calculated by FPLO coincides with the total energy obtained by the WIEN97 code within chemical accuracy, in the order of 1-2 mHartree per atom. This goal has been achieved by an efficient method to optimize the local basis states with respect to the total energy and by applying a shaping technique for the construction of densities and potentials.

After gathering enough experience with the first version of the code, that has been used and tested by about 10 individuals during the last two years, we decided to release the updated version FPLO®-2. Licences to use this version were issued to 15 groups during the workshop "Hands-on-FPLO" at IFW Dresden, held in the first week of March, 2002. The release includes a fast and convinient user interface and several tools to process output data. Informations on the workshop and on the licence conditions can be obtained from our homepage, **http://www.ifw-dresden.de/FPLO/**.

Before we proceed to present the background of the method and some of the obtained results, a few words should be spent on the history of this development. The ancestor of our present method is the linear combination of atomic orbitals method (LCAO), well-known from textbooks and, besides the complementary plane-wave method, most frequently explained to students in solid state physics. LCAO has two major disadvantages. At first, many Slater-Koster integrals have to be calculated since the atomic functions are far-ranging. Second and more severe, the atomic basis is incomplete if only bound states are included. In the mid-seventies, Helmut Eschrig started to develop an optimized LCAO method being exempt from the mentioned short-comings. The trick was to smoothly localize the atomic orbitals by an attractive potential [2]. The same idea is used in the present code in refined form, see Section . The ins and outs of

---

[1]On purpose, we do not quote the individual methods: to forget one of them would be worse than not to mention any...

Optimized LCAO were published in in the year 1988 together with calculated data for all light metals of the periodic table up to Zn [3].

As time went by, the calculation of band structures and densities of states alone was not sufficient anymore, and total energy calculations came into focus. Optimized LCAO could not compete in this field, since it relied on a representation of radial functions (wave functions, densities, and potentials) in terms of Slater-type orbitals. This choice had been taken on the background of the available main storage (up to at most 1 MByte) of computers accessible to Dresden physicists before 1990. In the early nineteeth, it became clear by attempts of Ulrike Nitzsche that the Slater-type representation had to be abandoned. In addition, we were heading for uttermost accuracy. Thus, Arthur Ernst in our group implemented a mixed basis scheme that achieved this goal at the price of a comparably poor performance [4]. The accuracy obtained by this method is perhaps not surpassed yet, but it cannot be used for elementary cells larger than a few atoms. On the basis of the existing experience, Klaus Koepernik developed the current scheme. It perhaps represents the best compromise between absolute accuracy and performance [1].

The described development through more than two decades was almost from the beginning paralleled by the implementation of important extensions to the basic codes. Chemical disorder could be treated in the optimized LCAO code within non charge-selfconsistent CPA, implemented by the late Reinhard Richter in collaboration with Bedrich Velický [5]. A much extended and completely charge-selfconsistent CPA version [6, 7] was added to FPLO by Klaus Koepernik on the basis of the nearly forgotten pseudo-spin approach of Blackman, Esterling, and Berk. Relativistic versions of both codes have been developed as well, by Manuel Richter for the old code [8, 9] and, quite recently, by Ingo Opahle for FPLO [10]. Both implementations are based on the full four component representation of the Bloch states. Finally, LSDA+U is just about to be completed by Igor Chaplygin.

What remains to be said is organized in the following way. The next section compiles the principles of FPLO in more detail. Sections , , and describe the implementations of CPA, LSDA+U, and the relativistic versions, respectively. The content, the performance, and the portability of the present release, FPLO®-2, are briefly outlined in Section . Finally, Section brings the summary and the outlook.

Principles of FPLO

Local-Orbital Minimum-Basis Scheme

We start from the well-known ansatz for the Bloch states $\psi_{\mathbf{k}n}(\mathbf{r})$,

$$\psi_{\mathbf{k}n}(\mathbf{r}) = \frac{1}{\sqrt{N}} \sum_{\mathbf{R}\mathbf{s}L} \phi_{\mathbf{s}L}(\mathbf{r} - \mathbf{R} - \mathbf{s}) C_{L\mathbf{s},\mathbf{k}n} e^{i\mathbf{k}(\mathbf{R}+\mathbf{s})} \ . \tag{1}$$

The basis states $\phi_{\mathbf{s}L}$ used to approximate the Kohn-Sham wave function of the crystal are local orbitals centered at sites $\mathbf{s}$ in the elementary cell defined by the lattice vector $\mathbf{R}$. They are solutions of an atom-like Schrödinger equation and are denoted by a complete set of atomic quantum numbers $L = \{\rho, l, m\}$.

The secular equation to be solved is

$$HC = SC\epsilon \,, \tag{2}$$

since the basis is nonorthogonal. Hamiltonian and overlap matrices are defined according to

$$H_{\mathbf{s}'L',\mathbf{s}L} = \sum_{\mathbf{R}} \langle \mathbf{0s}'L'|\hat{H}|\mathbf{R s}L \rangle e^{i\mathbf{k}(\mathbf{R}+\mathbf{s}-\mathbf{s}')}, \tag{3}$$

$$S_{\mathbf{s}'L',\mathbf{s}L} = \sum_{\mathbf{R}} \langle \mathbf{0s}'L'|\mathbf{R s}L \rangle e^{i\mathbf{k}(\mathbf{R}+\mathbf{s}-\mathbf{s}')}. \tag{4}$$

As usual, the local basis states are divided into two classes, the core states $\phi_{\mathbf{s}L_c}$ and the valence states $\phi_{\mathbf{s}L_v}$, to avoid unnecessarily large matrix problems. We define the core states by

$$\langle \mathbf{R}'\mathbf{s}'L_c'|\mathbf{R s}L_c \rangle = \delta_{cc'}\delta_{\mathbf{R R}'}\delta_{\mathbf{s s}'} \,. \tag{5}$$

Provided this condition is fulfilled (in practice, to the requested level of accuracy), the core states can be removed from the basis by an exact transformation [4]. At first, we decompose the overlap matrix,

$$S = \begin{pmatrix} 1 & S_{cv} \\ S_{vc} & S_{vv} \end{pmatrix} = \begin{pmatrix} 1 & 0 \\ S_{vc} & S_{vv}^L \end{pmatrix} \begin{pmatrix} 1 & S_{cv} \\ 0 & S_{vv}^R \end{pmatrix} = S^L S^R, \tag{6}$$

where left and right triangular matrices S_{vv}^L and S_{vv}^R obey the relation

$$S_{vv}^L S_{vv}^R = S_{vv} - S_{vc}S_{cv} \,. \tag{7}$$

Further, by definition of the core states,

$$H = \begin{pmatrix} \epsilon_c 1 & \epsilon_c S_{cv} \\ S_{vc}\epsilon_c & H_{vv} \end{pmatrix}, \quad \epsilon_c = \mathrm{diag}(\cdots, \epsilon_{\mathbf{s}L_c}, \cdots). \tag{8}$$

Re-writing the secular equation,

$$(S^L)^{-1}H(S^R)^{-1}(S^R C) = (S^R C)\epsilon \tag{9}$$

leads us finally to the reduced problem

$$\tilde{H}_{vv}\tilde{C}_{vv} = \tilde{C}_{vv}\epsilon_v \,, \tag{10}$$

with the definition

$$\tilde{H}_{vv} = (S_{vv}^L)^{-1}(H_{vv} - S_{vc}H_{cc}S_{cv})(S_{vv}^R)^{-1} \tag{11}$$

and

$$C = \begin{pmatrix} 1 & -S_{cv}(S_{vv}^R)^{-1}\tilde{C}_{vv} \\ 0 & (S_{vv}^R)^{-1}\tilde{C}_{vv} \end{pmatrix}. \tag{12}$$

The orthogonality condition for the core states is controlled during the successive iterations and related warnings or error messages are displayed.

Basis Optimization

A crucial feature of the method is that the basis is readjusted at every iteration cycle and is optimized in the course of iteration. The core states obey the equation

$$\left(\hat{t} + v_{\mathbf{s}}^{\mathrm{at}}\right)\phi_{\mathbf{s}L_c} = \phi_{\mathbf{s}L_c}\epsilon_{\mathbf{s}L_c} \tag{13}$$

with $v_{\mathbf{s}}^{\mathrm{at}}$ being the crystal potential spherically averaged around the site center $\mathbf{s}$. The latter definition assures that a Bloch sum of the core orbitals and the related core eigenvalues $\epsilon_{\mathbf{s}L_c}$ are very good approximations to the solution of the true crystal Hamiltonian.

On the contrary, the valence orbitals are defined in the following way:

$$\left(\hat{t} + v_{\mathbf{s}}^{\mathrm{at}} + \left(\frac{r}{r_{\mathbf{s}L_v}}\right)^4\right)\phi_{\mathbf{s}L_v} = \phi_{\mathbf{s}L_v}\epsilon_{\mathbf{s}L_v} \tag{14}$$

with $r_{\mathbf{s}L_v} = (r_{\mathrm{NN}}(\mathbf{s})x_{0L_v}/2)^{\frac{3}{2}}$, where r_{NN} is the nearest neighbor distance and x_{0L_v} are dimensionless compression parameters. The seemingly strange scaling of the $r_{\mathbf{s}L_v}$ is the correct one for an empty lattice.

The effect of the additional confining potential is to compress the long-ranging orbital tails of the valence orbitals. The power law potential has minor influence on the orbital in the core region, while in the region far from the nucleus the orbitals undergo a drastic change, compared to solutions without the confining potential. To be precise, the valence orbitals are usually unbound states in the potential $v_{\mathbf{s}}^{\mathrm{at}}$ alone. A second, even more important effect of the valence orbital confinement is that the orbital resonance energies are pushed up to come close to the band centers, providing the optimum curvature of the orbitals (Figure 1).
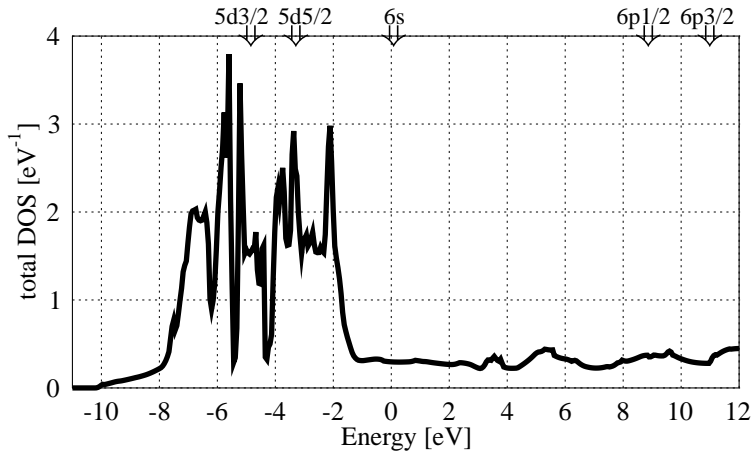

Figure 1: Total density of states of Au and the orbital energy positions $\epsilon_{\mathbf{s}L_v}$ of the optimized local basis states. All energies are relative to the Fermi level. (This figure has been produced with the relativistic FPLO code.)

The parameters x_0 enter the total energy via the basis expansion of the valence eigenstates. Therefore, the total energy is depending on x_0 as long as the basis set is incomplete. The most important feature of the FPLO basis treatment is that the total energy is minimized with respect to the set of compression parameters. In consequence, FPLO is not a fixed basis scheme.

In the self consistent calculation, the basis is adapted to the best x_0 set by using relations similar to the force theorem. One can prove the equality

$$\partial_{x_0} E^{\text{tot}} = \sum_{\mathbf{k}n}^{\epsilon_F} \partial_{x_0} \epsilon_{\mathbf{k},n} - \int n(\mathbf{r}) \partial_{x_0} V^{cr}(\mathbf{r}) d\mathbf{r} \tag{15}$$

using $\partial_{x_0} N = \int \partial_{x_0} n(\mathbf{r}) d\mathbf{r} \equiv 0$. The right-hand side of Eq. (15) turns out to be exactly zero for all x_0 if the basis orbitals form a complete set. Since the latter is obviously not the case, we require $\partial_{x_0} E^{\text{tot}}$ to vanish and obtain matrix equations for the calculations of the compression parameters, which then are solved simultaneously with the Kohn-Sham equations in every iteration step. This method turns out to be very efficient. A rule of thumb is that, depending on the starting values for x_0, a calculation with basis optimization takes only $1.5 \ldots 3$ times more iterations than without.

Partitioning of unity and shape functions

The representation of density and potential as locally finite lattice sums is achieved by using the partitioning of unity. Two types of shape functions are employed in FPLO.

(i) The overlap density is a lattice sum of terms, consisting of a product of two orbitals located at different lattice sites with a generalized occupation number. These terms have two cusps, one at each site. Each term is split into contributions from the two sites, which are "localized" at the corresponding site and fall off to zero at the other:

$$\phi_i n_{ij} \phi_j = f_{ij}(\mathbf{r}) \phi_i n_{ij} \phi_j + \phi_i n_{ij} \phi_j f_{ji}(\mathbf{r}) , \tag{16}$$

using 1D shape functions f_{ij} with the following properties

- $f_{ij}(\mathbf{r}) + f_{ji}(\mathbf{r}) \equiv 1 \quad \forall \mathbf{r}$

- $f_{ij}(\mathbf{s}_i) = f_{ji}(\mathbf{s}_j) = 1$

- f_{ij} is continuously differentiable to a certain degree

- f_{ij} behaves like $1 - O(|\mathbf{r} - \mathbf{s}_i|^N)$ and $O(|\mathbf{r} - \mathbf{s}_j|^N)$ at the site i and j respectively, with a certain order N

These properties assure that the function at one site will screen the cusp at the other site in a controlled manner.

One possible choice of shape functions is:

$$f_{ij}(\mathbf{r}) = p(x), \quad f_{ji}(\mathbf{r}) = p(1 - x) \tag{17}$$

with $x = (\mathbf{r} - \mathbf{s}_i)(\mathbf{s}_j - \mathbf{s}_i)/|\mathbf{s}_j - \mathbf{s}_i|^2$ and $p(x) + p(1 - x) \equiv 1$, $p(x) \equiv 1 \quad \forall \quad x \leq 0$ and $p(x) \equiv 0 \quad \forall \quad x \geq 1$. For the profile function $p(x)$ one may chose any function which fulfills
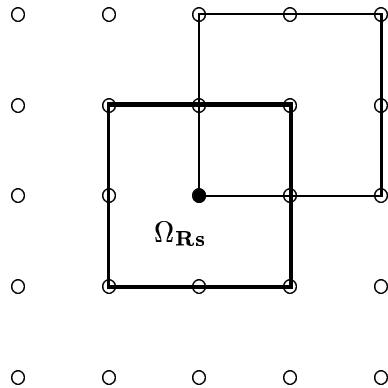
Figure 2: Overlapping Voronoi cells in a 2D square lattice.

the differentiability and power law conditions given above. Any such function creates a class of similar functions, generated by $p_n(x) = p(1 - p_{n-1}(x))$.

(ii) For the decomposition of the non-linear exchange and correlation potential into a sum of locally finite contributions we use a 3D shape function. The requirements for this functions are

- Each single shape function $f_i(\mathbf{r})$ is centered at a certain site $\mathbf{s}_i$

- $\sum_i f_i(\mathbf{r}) \equiv 1 \quad \forall \mathbf{r}$

- $f_i(\mathbf{r} - \mathbf{s}_i) \equiv 1 - O((\mathbf{r} - \mathbf{s}_i)^N)$

- The shape function at $\mathbf{s}_i$ (when multiplied with a lattice symmetric function) screens the singularities at all other lattice sites $\mathbf{s}_j$:
  $f_i(\mathbf{r} - \mathbf{s}_j) \equiv 0 + O((\mathbf{r} - \mathbf{s}_j)^N) \quad \forall j \neq i$

- f_i is continuously differentiable to a certain degree.

- The shape function has the "smallest possible compact support".

Our choice of shape functions is defined as follows. The most compact supports, which may be defined for every site in an arbitrary lattice are the Voronoi cells. Since the resulting shape functions should be overlapping, we chose Voronoi cells Ω with an eightfold volume compared to the standard definition. The distance between the central site and the defining boundary planes is two times larger than usual. Figure 2 shows overlapping Voronoi cells according to our definition in a 2D square lattice.

Each cell-defining plane is related to a certain neighboring site $\mathbf{s}_j$. For a given site $\mathbf{s}_i$, we define dimensionless scalar variables x_j and 1D profile functions h_j for every neighboring site $\mathbf{s}_j$, contributing to the cell boundary definition:

$$h_j(\mathbf{r}) = p(x_j), \quad x_j = \frac{(\mathbf{r} - \mathbf{s}_i)(\mathbf{s}_j - \mathbf{s}_i)}{|\mathbf{s}_j - \mathbf{s}_i|^2} \tag{18}$$

with an appropriately chosen profile $p(x)$:

107

- $p(0 + \delta) \equiv 1 - O(\delta^N)$

- $p(1 - \delta) \equiv 0 + O(\delta^N)$

- $p(x)$ continuously differentiable to a certain degree and monotonously decreasing

- $p(x) = 0, \quad x \geq 1$

- $p(x) = 1, \quad x \leq 0$

The product of all profile functions gives a cell-function

$$g_i(\mathbf{r}) = \prod_{\{j\}} h_j(\mathbf{r}) \,, \tag{19}$$

which excludes by its definition every lattice site except $\mathbf{s}_i$. Additionally, it falls off faster than a given power law, when approaching the cell boundary (and thus a neighbor site). The unity condition for the lattice sum of all shape functions is achieved by explicit normalization. Thus, the shape function reads

$$f_i(\mathbf{r}) = \frac{g_i(\mathbf{r})}{\sum g_i(\mathbf{r})} \,, \tag{20}$$

where the sum runs over all neighboring sites whose Voronoi cells overlap the cell at site $\mathbf{s}_i$. This is always a finite sum and it turns out that the numerical implementation of the shape functions described above is extremely efficient.

Density and Potential representation

Details of density and potential calculation have been published elsewhere [1]. Thus, we concentrate on the key points here.

The (spin) density in a non-orthogonal local basis scheme consists of net and overlap contributions. The former terms contain products of basis functions from the same site and are site-centered by construction. The latter terms contain products of basis functions from different sites. They are decomposed into site-centered contributions by application of the described partitioning technique. As a result, the total density is obtained as a lattice sum of site densities in spherical harmonics representation,

$$n(\mathbf{r}) = \sum_{\mathbf{Rs},lm} n_{\mathbf{s},lm}(|\mathbf{r} - \mathbf{R} - \mathbf{s}|) Y_{lm}(\mathbf{r} - \mathbf{R} - \mathbf{s}) \,. \tag{21}$$

The maximum l-numbers used are 6 for the net contributions (by construction from states of $l_{\max} = 3$) and 12 for the overlap contributions.

The Hartree potential is evaluated with the help of Ewald's method applied to all multi-pole components. While the local part can be used 'as is', the Fourier-transformed contribution is inserted into the 3D partitioning-mill described in the previous section. This again provides us with a locally finite lattice sum. Finally, the xc potential is partitioned in exactly the same way, and the local contributions to the crystal potential are expanded into spherical harmonics,

$$V^{cr}(\mathbf{r}) = \sum_{\mathbf{Rs},lm} v_{\mathbf{s},lm}(|\mathbf{r} - \mathbf{R} - \mathbf{s}|) Y_{lm}(\mathbf{r} - \mathbf{R} - \mathbf{s}) \,. \tag{22}$$

Now, when it comes to evaluate the multi-center Slater-Koster integrals, we can joyfully harvest the fruits of our endeavors. As the extension of all involved functions is finite and restricted to few neighbor atoms, relatively few integrals have to be calculated, and no cut-off is needed. The one- and two-center integrals are further simplified by the application of angular momentum rules to one- and two-dimensional numerical integrations, respectively. All integration meshes are tuned to achieve accuracies of better than 1 μHartree in the Hamiltonian integrals and better than 10^{-6} in the overlap integrals.

Coherent Potential Approximation (CPA) for partial substitutional disorder

The density- and potential representation as well as the local orbital basis set used in FPLO are well suited to apply a variant of the CPA to describe disordered bulk materials. For this purpose we employ a generalization of the Blackman-Esterling-Berk (BEB) matrix-CPA. This version of CPA provides a scattering theory in matrix notation, which parallels the usual KKR-formulation. In contrast to all other simple types of matrix CPA, the BEB-CPA does not restrict the values of the Hamiltonian matrix elements. It completely incorporates the off-diagonal disorder effects. Moreover, the BEB-CPA has been proven to fulfill the dilute or single impurity limit.

The main ingredients and approximations are sketched in the following. The random occupation of the lattice sites is described by assigning pseudo spins to every site, labeled by the atom sorts, which may occupy the site under consideration. They take values 1 or 0, depending on the occupation of the site. This treatment is flexible and allows the description of partial disorder. We assume statistical independence of pseudo spins from different sites, thus neglecting short range order effects.

The main assumption is the linear dependency of all real space functions (density, potential, and orbitals) on the pseudo spins. In this way it is possible to write down density, potential, Hamiltonian, and Green's function as pseudo spin dependent random objects, which model a statistical ensemble. For a certain member of the ensemble, say a particular realization of all pseudo spins, these objects become nonrandom and represent the behavior of exactly this member.

The random Hamiltonian and Green's matrix are defined in an enlarged Hilbert space (due to the pseudo spin degrees of freedom), which to a certain extent describes the true statistical ensemble. The equation of motion for the Green's function is formulated in this Hilbert space. One can write down the scattering matrix for this equation and ends up with a CPA condition, which defines an averaged Green's matrix in the enlarged space. It is possible to show, that the matrix elements of this averaged Green's function represent relevant partially averaged physical quantities like generalized occupation numbers, which enter the density expression.

In practical calculations, the CPA condition is solved within the single site approximation (the scattering matrix is decoupled into single site events and the CPA-condition is applied to the single site scattering matrices only). The second simplification is done for the occupation numbers entering the density expression. It is assumed, that the true (random) occupation numbers

may be replaced by conditional averages with only the sites indexing the occupation numbers being kept random. The resulting density expression is again linearly depending on the pseudo spins and, thus, all ingredients for a charge self-consistent calculation are defined.

The CPA method, as shortly outlined above, has been applied to the FeAl system. This system undergoes several structural and magnetic phase transitions in dependence of concentration and temperature. The iron rich site of the phase diagram consists of structures, derived from the bcc structure. All atoms are at bcc sites, but the occupation is partially disordered (experiments provide evidence for partial long range order). Depending on the actual occupation one may describe the resulting structures by superstructures of the bcc lattice, where some sub-lattices are occupied with iron or aluminum only, while the other sub-lattices may be occupied randomly by iron and aluminum. Three possible structures are the A_2 structure (completely disordered bcc lattice), the B_2 structure (CsCl structure with one sub-lattice randomly occupied), and the DO_3 structure (four sub-lattices, one or two occupied randomly, depending on the aluminum concentration.)
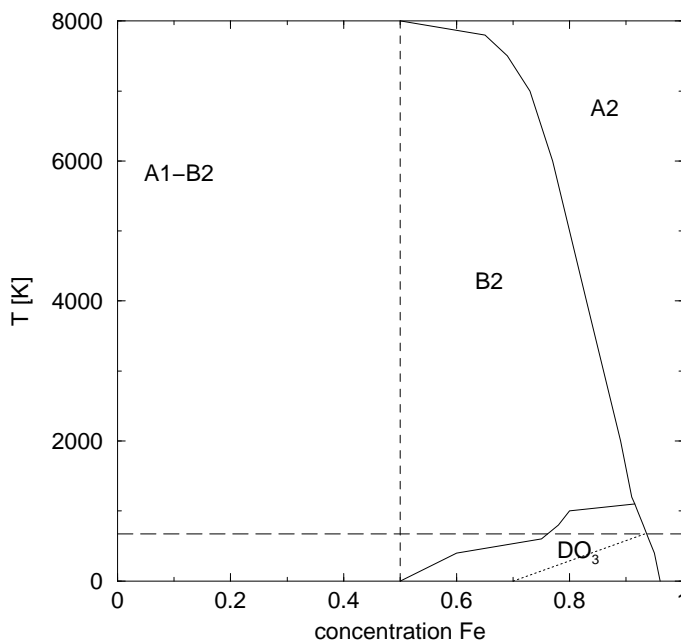

Figure 3: Theoretical phase diagram of Fe-Al.

We have investigated the influence of the types of partial disorder on the magnetic and mechanical properties. For every structure type and concentration we optimized the lattice constant. The resulting energy surface was combined with a simple mixing entropy term to provide an estimate for the enthalpy. From this we concluded a rough picture of the phase diagram at the iron rich side, Figure 3. In the Fe concentration range $50\% - 96\%$ the DO_3 phase has the lowest enthalpy at low T. Above 90% Fe, the A_2 phase replaces the DO_3 phase when temperature increases, while below 90% Fe concentration, the DO_3 phase is replaced by the B_2 phase. Above 70% the enthalpy curve is concave, which indicates de-mixing and instability of the DO_3 and B_2 phases.

Experiments indicate only a ... concentration ... ound 70% Fe, where a DO$_3$ ... is stable. ... contradicts our ... ng of a stable D ... se extending over a larger con ... ion range. We believe that the experimentally observed B$_2$ phase is a thermodynamically meta-stable phase, res ... rom freezing ... exchange when cooling down the sampl ... the other hand, the e ... py difference bet ... B$_2$ phase and DO$_3$ phase becomes rathe ... for concentrations close to 50% F ...

There ... er quantities ... ng the stabil ... he DO$_3$ phase found in our calculation. The first result concerns th ... brium volume a ... ro temperature. Starting from pure iron, the lattice volume is linearly increasing with the aluminum concentration. Around 70% Fe the volume stays more or less constant while for still lower Fe concentrations the volume is further increasing. This behavior is exactly reproduced in the spin polarized DO$_3$ phase calculations. The reason for this finding is a magneto-strictive effect. In the same region where the lattice constant is staying constant the magnetic moment strongly decreases with increasing Al content. We have found two minima in the total energy versus the magnetic moment. Depending on the lattice constant, one of the two minima is stable. This could provide a simple mechanism of magneto-striction. As a final note, the B$_2$ phase shows similar behavior, but the DO$_3$-phase magnetization and volume versus concentration curves are resembling the experimental findings more closely.

LSDA+U

We have implemented the LSDA+U approximation for computing the electronic structure of compounds with strong correlations, such as transition metal oxides. It is well known that LSDA often fails to describe the transport and magnetic properties of such compounds. The reason for this failure is primarily an insufficient description of the on-site Coulomb correlation of the d-electrons. LSDA+U proves to give better results in many cases.
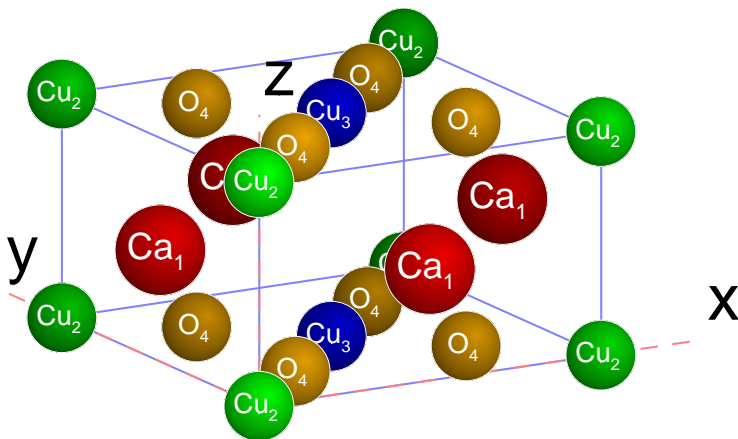
Figure 4: Antiferromagnetic unit cell of CaCuO$_2$. Note that the cell is rotated by $\pi/4$ about the Z-axis with respect to the standard CuO$_2$ plaquett, so that the d_{xy} copper orbital is involved in σ-bonding with in-plane p-orbitals of the neighboring oxygen atoms.

The implemented version of LSDA+U is rotationally invariant and has few free parameters (Slater integrals). In the considered d-systems, we restrict the number of parameters to the Coulomb U and exchange J interaction constants. Under fixed choice of the parameters and well-defined d-orbitals the LSDA+U ground-state energy is a functional of spin-density, which puts a rigorous ground for using it in the framework of DFT. The chosen form of the double-counting term ensures that the functional reduces to that of LSDA in the limiting cases of full or zero occupation of the relevant shell.

As an example, results for the compound $CaCuO_2$ are presented. This compound does not exist in nature in the pure form but can be stabilized by substituting about 14% of Ca by Sr. The idealized crystal $CaCuO_2$ has simple tetragonal structure and is made up of CuO_2 planes separated by Ca layers. The elementary cell of $CaCuO_2$ with chessboard-ordered antiferromagnetic arrangement is shown in Fig. 4. The lattice constants $a = 5.46$ Å and $c = 3.20$ Å were used in the calculations.

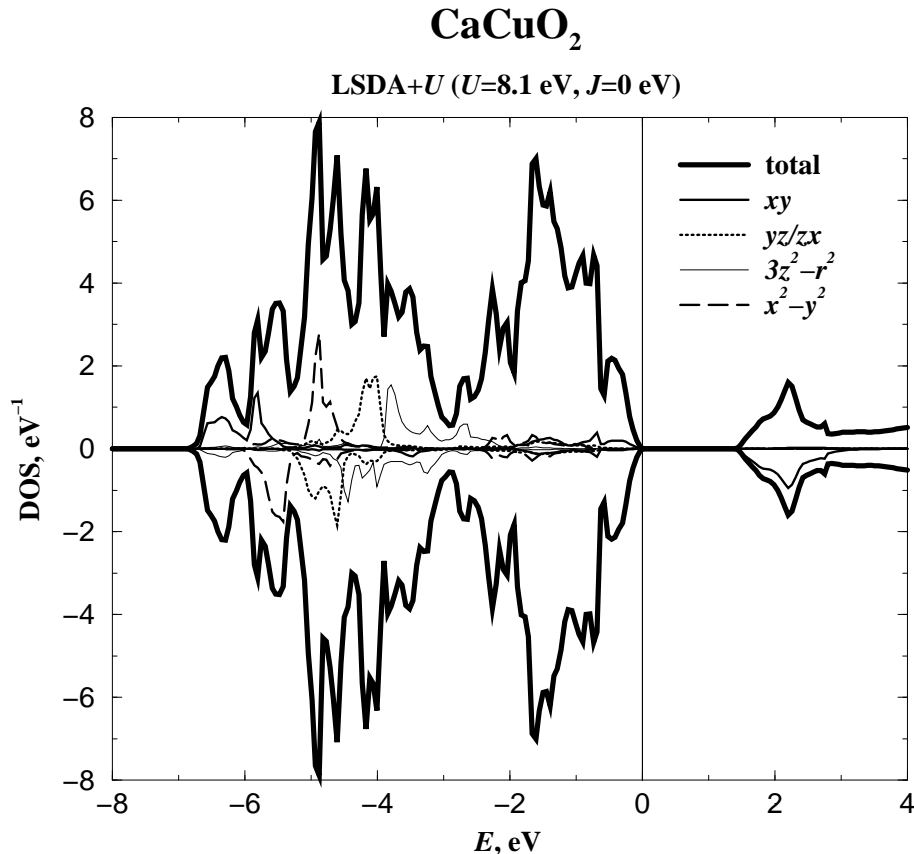Figure 5: Density of states of antiferromagnetic $CaCuO_2$ projected on d-orbitals of a copper atom. The majority and minority spin channels are drawn above and below the X-axis, respectively. Empirical values $U = 8.1$ eV and $J = 0$ eV are used.

LSDA predicts the compound to be a paramagnetic metal, though its existing counterpart $Ca_{0.86}Sr_{0.14}CuO_2$ is an antiferromagnet with large insulating gap, the influence of the Sr substitution impurity on the electronic structure being negligible.

The implemented LSDA+U version yields the correct insulating ground state. The values of the magnetic spin moment, 0.71 μ_B per Cu atom, and the width of the gap, 1.44 eV, are close to the

112

experimental values (total moment 0.51 μ_B per Cu atom and gap width 1.5 eV). The computed density of states projected on d orbitals of a copper atom is shown in Fig. 5. One notes that one d_{xy}-orbital ($d_{x^2-y^2}$ in standard notation) is unoccupied and split off the rest Cu-3d/O-2p complex.

Relativistic Versions

Four component relativistic FPLO

Our aim is to solve the Kohn-Sham-Dirac equation in local spin density approximation (LSDA),

$$\hat{H}|\mathbf{k}n\rangle = \left[-ic\alpha\nabla + \beta c^2 + V^{cr} + \beta\Sigma_z B^{cr}\right]\,|\mathbf{k}n\rangle = \epsilon|\mathbf{k}n\rangle\,, \tag{23}$$

with the XC-field $\mathbf{B} \equiv B^{cr}\hat{z}$ treated in a collinear approximation and aligned along the (arbitrary) $\hat{z}$-axis,

$$B^{cr}(\mathbf{r}) = \frac{1}{2}\left(V_{xc}^{+}[n,m] - V_{xc}^{-}[n,m]\right)\,. \tag{24}$$

As usual, the effective crystal potential, V^{cr}, in equation (23) contains the Hartree potential, the external potential V and the exchange and correlation potential V_{xc},

$$V^{cr}(\mathbf{r}) = \int \frac{n(\mathbf{r}')}{|\mathbf{r}-\mathbf{r}'|}\,d^3r' - \sum_{\mathbf{Rs}} \frac{Z_\mathbf{s}}{|\mathbf{r}-\mathbf{R}-\mathbf{s}|} + \frac{1}{2}\left(V_{xc}^{+}[n,m] + V_{xc}^{-}[n,m]\right)\,. \tag{25}$$

Further, c denotes the velocity of light, and α, β and Σ_z are the usual 4×4 Dirac and Pauli matrices. In contrast to most other relativistic band structure methods we solve equation (23) in a four component formalism, thus avoiding further approximations like the second variation treatment.

The scheme presented here is a relativistic extension of the non relativistic FPLO scheme described in Section 2 and is built on the same numerical grounds, thus enabling us to study the influence of relativistic effects within one and the same highly accurate scheme. To stress this opportunity, we mention that the total energies obtained by the non relativistic FPLO code and by the RFPLO code in a quasi non relativistic mode ($c = 10^6$) agree within some μHartree even for heavy elements like Au, with the main deviations stemming from the 1s electrons. The scalar relativistic implementation (SRFPLO) is briefly described in the second part of this section.

The same kind of ansatz for the Bloch states as in the non relativistic version is used,

$$|\mathbf{k}n\rangle = \sum_{\mathbf{Rs}\nu} \frac{1}{\sqrt{N}} C_{\nu\mathbf{s},\mathbf{k}n}\,|\mathbf{Rs}\nu\rangle\,e^{i\mathbf{k}(\mathbf{R}+\mathbf{s})}\,, \tag{26}$$

but now in terms of localized four-spinors $|\mathbf{Rs}\nu\rangle$. The label $\nu = (\rho,\kappa,\mu)$ denotes a complete set of atomic quantum numbers in relativistic notation. The chosen ansatz includes only electron-like spinors with the ratio between large and small components determined in the preceding solution of atomic-like problems. This ensures (i) minimum size of the matrix, namely twice the size of the non relativistic problem and (ii) a restriction of the solutions to the electron sector of the Hilbert space.

For our minimum basis scheme, the optimum choice of the local basis states $|\mathbf{R}s\nu\rangle$ is crucial for highly accurate and efficient calculations. In analogy to the non relativistic FPLO scheme, we define the local basis states as solutions of a single particle Dirac equation

$$\left[-ic\alpha\nabla + \beta c^2 + v_{\mathbf{s}\nu}^{at} + \beta\Sigma_z B_{\mathbf{s}\nu}^{at}\right]\phi_{\mathbf{s}\nu} = \pm\phi_{\mathbf{s}\nu}(\epsilon_{\mathbf{s}\nu} + c^2) \tag{27}$$

in a spherical, orbital dependent potential

$$v_{\mathbf{s}\nu}^{at}(|\mathbf{r} - \mathbf{s}|) = v_{\mathbf{s}}^{at}(|\mathbf{r} - \mathbf{s}|) + V_{\rho l}^{\text{conf}} = \frac{1}{4\pi}\int d\Omega\, V^{cr}(\mathbf{r} - \mathbf{s}) + \delta_{\nu v}\frac{1+\beta}{2}\left(\frac{|\mathbf{r} - \mathbf{s}|}{r_{0,\rho l}}\right)^4 \tag{28}$$

which is the sum of the spherically averaged crystal potential, $v_{\mathbf{s}}^{at}$, and an additional confining potential term that is only applied to valence states (denoted by the symbolic writing $\delta_{\nu v}$). Further, the spherically averaged crystal XC-field is included,

$$B^{at}(|\mathbf{r} - \mathbf{s}|) = \frac{1}{4\pi}\int d\Omega\, B^{cr}(\mathbf{r} - \mathbf{s}). \tag{29}$$

For the solution of equation (27) we neglect the magnetic coupling terms of order $O(1/c^2)$ [11] and take an ansatz

$$\phi_{\rho\kappa\mu}(\mathbf{r}) = \begin{pmatrix} g_{\rho\kappa\kappa\mu}(r)\chi_{\kappa\mu}(\hat{r}) \\ if_{\rho\kappa\kappa\mu}(r)\chi_{-\kappa\mu}(\hat{r}) \end{pmatrix} + \begin{pmatrix} g_{\rho\kappa\tilde{\kappa}\mu}(r)\chi_{\tilde{\kappa}\mu}(\hat{r}) \\ if_{\rho\kappa\tilde{\kappa}\mu}(r)\chi_{-\tilde{\kappa}\mu}(\hat{r}) \end{pmatrix} \tag{30}$$

with $\tilde{\kappa} = -\kappa - 1$ and spherical spinors

$$\chi_{\kappa\mu}(\hat{r}) = \begin{pmatrix} c_{\kappa\mu\uparrow}\mathcal{Y}_{l_\kappa\mu-\frac{1}{2}}(\hat{r}) \\ c_{\kappa\mu\downarrow}\mathcal{Y}_{l_\kappa\mu+\frac{1}{2}}(\hat{r}) \end{pmatrix} \tag{31}$$

where the $\mathcal{Y}_{lm}$ are complex spherical harmonics and the $c_{\kappa\mu\sigma}$ are Clebsch-Gordan coefficients. This ansatz gives rise to a set of four coupled differential equations, except for the case $|\mu| = l_\kappa + \frac{1}{2}$. In the case of a non magnetic calculation, the ansatz (30) reduces to

$$\phi_{\rho\kappa\mu}(\mathbf{r}) = \begin{pmatrix} g_{\rho\kappa}(r)\,\chi_{\kappa\mu}(\hat{r}) \\ if_{\rho\kappa}(r)\,\chi_{-\kappa\mu}(\hat{r}) \end{pmatrix} \tag{32}$$

giving rise to two coupled equations. For both types of equations, a number of numerical standard methods exist, such as Runge-Kutta or multi step methods. We use a predictor corrector method of Adams-Bashford-Moulton type.

The numerical effort of a local-basis method is determined by the size of the matrix on the one hand, and by the number of multi center integrals on the other hand. We have already discussed the matrix size, being twice as large as in the non relativistic approximation. For small elementary cells and moderate numbers of $\mathbf{k}$ points, however, the numerical effort is primarily determined by the multi center integrals. Given a certain geometry, it depends mainly on the number of different radial functions we have to consider. Consider at first non magnetic calculations. Here, we have roughly twice the number of radial functions for the large components (due to the $j = l \pm \frac{1}{2}$-splitting of states with $l > 0$) compared to the non relativistic approach, enhancing the effort to calculate Slater-Koster integrals by a factor of $3\ldots4$. The same holds true for the small components, giving another factor of two for the total effort. This is still tractable and *can also be done with the actual RFPLO code.*

However, in standard calculations we take advantage of the fact that the small components are virtually *confined within half of the nearest neighbor distance*, so that we can neglect all the multi center integrals between small components. With this approximation we save a factor of two both in the calculation time and memory, while allowing for a tiny error in the absolute value of the total energy. It is of the order of 50 μHartree per atom for gold, much smaller than our accuracy demands (Figure 6).
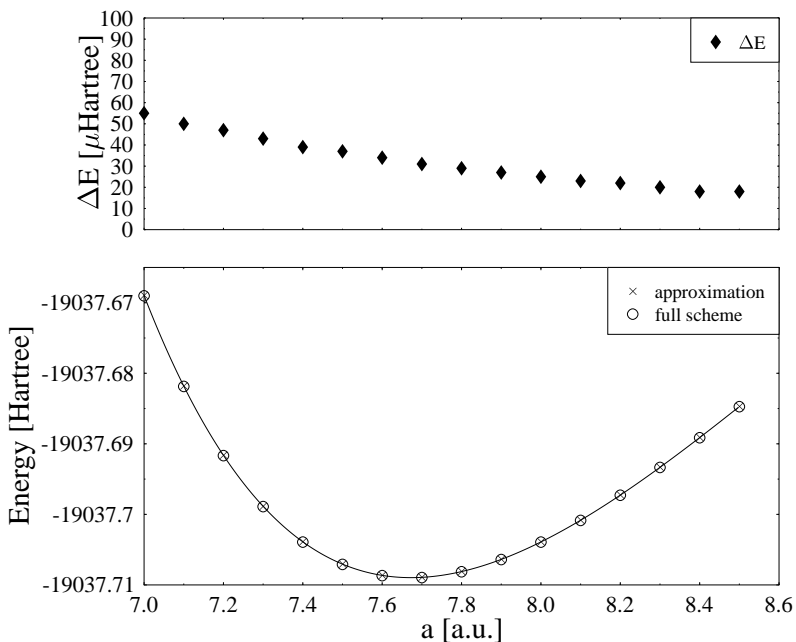

Figure 6: Total energy of Au versus lattice constant, using the Perdew-Wang 92 version of LDA and a minimum valence basis including 5p, 6s, 6p, and 5d states. Results obtained by including and excluding the overlap between small components on different sites are compared. The related energy difference is shown in the upper panel at enlarged scale.

In the case of magnetic calculations, the method is tedious if no additional approximations are made. For a d-shell, e.g., there are ten states with different energies, each of them having two different radial wave functions (except for the $\mu = \pm\frac{5}{2}$-states) for the large components. Taking into account the small components as well, we easily arrive at a factor of 10^3 for the numerical effort, in comparison with the non relativistic situation. We thus introduce the following approximative scheme which also allows calculations for more complicated structures with an acceptable accuracy. Again, the code allows to switch off the described approximation to allow full control of the accuracy at the price of enhanced computational effort.

For each (ρ, l)-shell the radial functions of the large components are approximated by a linear combination of two radial functions

$$g_{\rho\kappa\mu\sigma} \approx c_{\rho\kappa\mu\sigma}g_{\rho l} + \tilde{c}_{\rho\kappa\mu\sigma}\tilde{g}_{\rho l}. \tag{33}$$

This approach is exact in the two limiting cases of vanishing spin polarization or vanishing spin-orbit interaction. The coefficients $c_{\rho\kappa\mu\sigma}$ and $\tilde{c}_{\rho\kappa\mu\sigma}$ are determined in such a way that the

expression

$$\|g_{\rho\kappa\mu\sigma} - (c_{\rho\kappa\mu\sigma}g_{\rho l} + \tilde{c}_{\rho\kappa\mu\sigma}\tilde{g}_{\rho l})\| \tag{34}$$

is minimized. For the functions $g_{\rho l}$ and $\tilde{g}_{\rho l}$ we take the (normalized) radial wave functions of the large components belonging to the state with the highest and lowest energy of the specific (ρ, l)-shell. The scheme is written quite general, so that an approximation with a larger set of functions would not pose any problem. In all cases tested so far, the influence of the present approximation on the total energies was well below 100 μHartree per atom. The effect on relative energy differences like magneto-crystalline anisotropy energies (MAE) is tiny and can be neglected in comparison with other sources of errors like the finite **k**-mesh. This insensitivity is reasoned by the little effect of a rotation of magnetization direction on the size of the spin moment (apart from heavy elements, where the MAE is large).

Scalar Relativistic FPLO

For many applications, an approximate consideration of relativistic effects is sufficient. Spin-orbit coupling is neglected in so-called scalar relativistic approaches, so that wave functions with non-relativistic symmetry are obtained. There is, however, no unique definition of a scalar relativistic approximation possible. Frequently used schemes are those due to Koelling and Harmon [12] or Douglas, Kroll, and Hess, employed in Reference[13].

Our approach does not rely on solving an explicit scalar-relativistic equation but rather on averaging the large components and related energies of the local orbitals. It was previously implemented in the relativistic OLCAO method [8]. The advantage over other scalar relativistic schemes is an enhanced accuracy of the charge density close to the atomic nuclei and a smaller difference of the total energy from fully relativistic calculations.

Neglecting spin dependence for the sake of simplicity, we define scalar relativistic local basis states $|\mathbf{R}sL)$ by

$$\tilde{H}^{at}|\mathbf{R}sL) = \tilde{\epsilon}_{\mathbf{s}\rho l}|\mathbf{R}sL) \tag{35}$$

$$(\mathbf{r}|\mathbf{R}sL) = f_{\mathbf{s}\rho l}(r)\,Y_{lm}(\hat{r}) \tag{36}$$

as solutions of a fictitious spherical Hamiltonian $\tilde{H}^{at}$ with non-relativistic symmetry. The scalar relativistic radial wave functions

$$f_{\mathbf{s}\rho l}(r) = \frac{1}{\mathcal{N}}\sum_{j=l\pm\frac{1}{2}}\sum_{\mu=-j}^{j} g_{\mathbf{s}\rho\kappa(j)}(r) \tag{37}$$

are defined by averaging over the large components of all states of a (ρ, l)-shell, with a normalization factor $\mathcal{N}$. The scalar relativistic one particle energies

$$\tilde{\epsilon}_{\mathbf{s}\rho l} = \frac{1}{4\,l+2}\sum_{j=l\pm\frac{1}{2}}\sum_{\mu=-j}^{j} \epsilon_{\mathbf{s}\rho\kappa(j)} \tag{38}$$

are also averaged over the spin orbit split energies of a (ρ, l)-shell. The scalar relativistic Hamiltonian $\tilde{H}^{at}$ is defined only implicitly by Eqs. (35), (37) and (38).

The remaining treatment of the valence states completely parallels the non-relativistic version, while core states are treated in the same way as in a relativistic calculation.
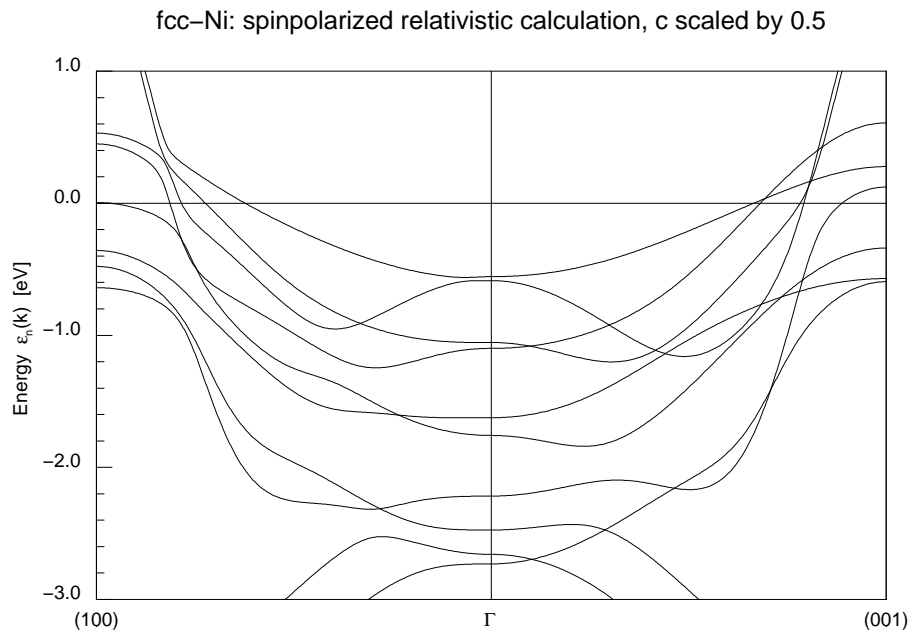
Examples

fcc–Ni: spinpolarized relativistic calculation, c scaled by 0.5

Figure 7: Band structure of ferromagnetic fcc-Ni. The velocity of light was scaled by a factor 0.5.
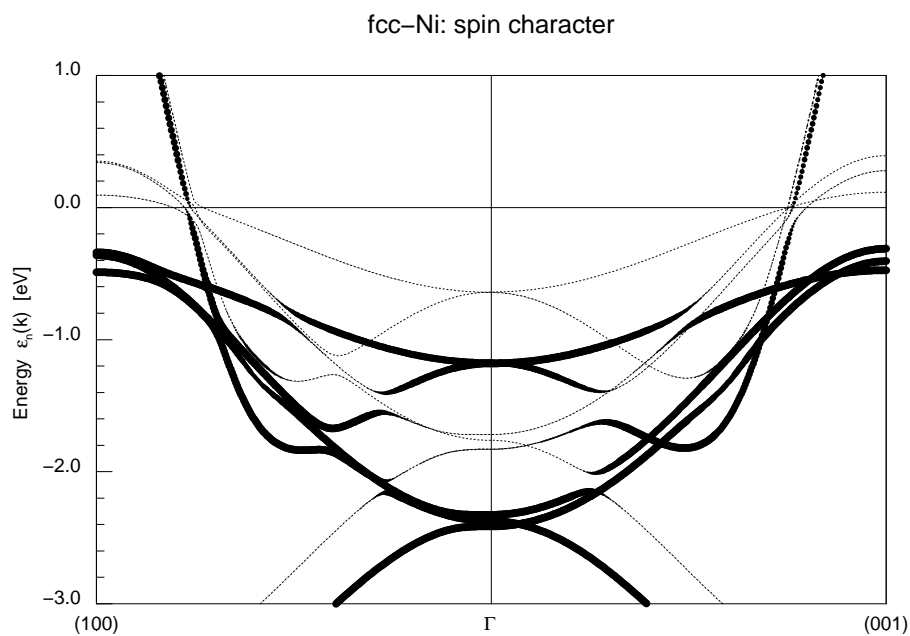

fcc–Ni: spin character

Figure 8: Band structure of ferromagnetic fcc-Ni with the spin character indicated by the size of the points. The largest size corresponds to pure majority spin character, while the smallest size corresponds to pure minority spin character.

Band structure of fcc-Ni: Lifting of degeneracies and spin characters

In the non-relativistic theory, the symmetry of the fcc-lattice implies degeneracies of the band

structure at points of high symmetry like the Γ-point. Relativistic effects usually lead to a reduction of symmetry in ferromagnetic metals. As a consequence, the corresponding representations of all one atomic lattices become one-dimensional [14] and group theoretical arguments do no longer imply degeneracies of the band structure, with the remaining degeneracies being accidental. On an intuitive level this fact may be understood if one lets the lattice constant go to infinity: The symmetry is still the same, but the bands become flat with energies corresponding to the atomic levels, which are non-degenerate. As an example, a band structure of fcc-Ni is shown in Fig. 7. To emphasize the effect, the bands drawn are taken from a calculation with the velocity of light set to $c/2$.

Another effect implied by the relativistic theory is that the spin is no longer a good quantum number. Thus a simple splitting into spin up and spin down bands is not appropriate anymore. However, a projection onto spin states as demonstrated in Fig. 8 can be useful.

Equilibrium lattice constant of thorium

The evaluation of equilibrium lattice parameters is one of the fundamental goals of density functional calculations. It is, within a given approximation of the xc functional, a well-defined task and ideal for comparing the reliability of different numerical methods.
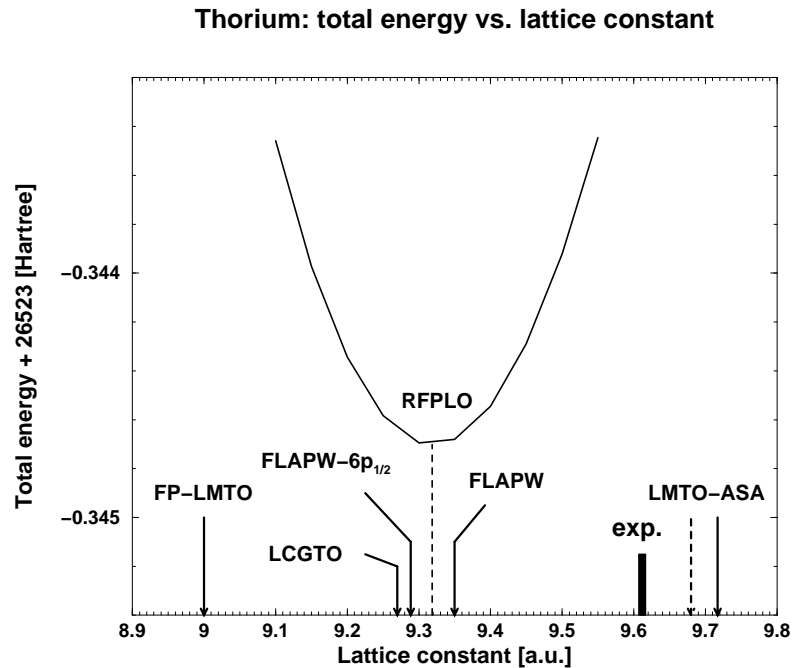
Thorium: total energy vs. lattice constant

Figure 9: Equilibrium lattice constant of thorium: comparison of experimental data and LDA results obtained by different numerical schemes.

Figure 9 shows the dependence of the total energy of fcc thorium on the lattice constant obtained with RFPLO using the Perdew-Wang 92 LDA [15]. The position of the minimum is indicated by a dashed line. Further, the experimental lattice constant is given by a box, where the width shows the scatter of experimental data from Pearson's table. Equilibrium lattice constants obtained by five different methods are denoted by arrows: LMTO-ASA [16]; FP-LMTO [17];

LCGTO-FF and FLAPW [18]; FLAPW-$6p_{1/2}$ (unpublished data obtained as described in Ref. [19]).

The value obtained by LMTO-ASA refers to room temperature [16], but the related zero-temperature value (dashed line, estimated from the linear coefficient of thermal expansion) is not so much below the former one. At the first glance, one could be happy with LMTO-ASA, yielding a result quite close to (but above!) the experiment. If we turn to the full-potential version, FP-LMTO, that should provide a numerically more accurate result by definition, it becomes clear that ASA is not suited for a quantitative analysis of lattice geometries.[2] Note, that both calculations used the same version of LDA (Hedin-Lundqvist) and included spin-orbit coupling in the so-called second variational step [20]. The latter method suffers from convergence problems of the employed basis of spin eigenstates [21]. Careful convergence of this basis in an FLAPW calculation [18] yields a result about 2.5% below the experimental value, as commonly obtained in LDA. In the same publication, LCGTO-FF results were presented. This method uses an approximation for the full Dirac equation different from the second variational step. As pointed out in Ref. [18], both calculations should provide approximate upper and lower bounds, respectively, for the spin-orbit effects.

Going to still more accurate treatments of spin-orbit coupling, we indeed find results between the latter two. Local $6p_{1/2}$-states were included in FLAPW recently [19], thus reducing the convergence problem of the spin eigenstate basis considerably (FLAPW-$6p_{1/2}$). Finally, the RFPLO result is given (curve and dashed line), were spin-orbit coupling is exactly treated in the limits of the Kohn-Sham-Dirac equation.

It is quite satisfactory that the results of the two most accurate methods are close to each other (though not yet as close as the different experiments) and between the bounds provided by LCGTO-FF and FLAPW. Such a level of reproducibility with completely different numerical methods can provide a save basis for the development of improved xc functionals.

FPLO-2

The latest version of the code, FPLO®-2, has been released recently.[3] Licenses for using the code are issued for a moderate fee. You can find the related conditions at the FPLO homepage, **http://www.ifw-dresden.de/FPLO/**. We distribute the release by email. It consists of source code in Fortran and C and a short documentation. The scalar relativistic version of FPLO is included in FPLO®-2, but not the fully relativistic one. In the course of the year 2002, we intend to distribute an update with the CPA and LSDA+U options, both included in the present license.

---

[2]We would like to emphasize, however, that a number of important qualitative results has been obtained by this efficient method in the past.

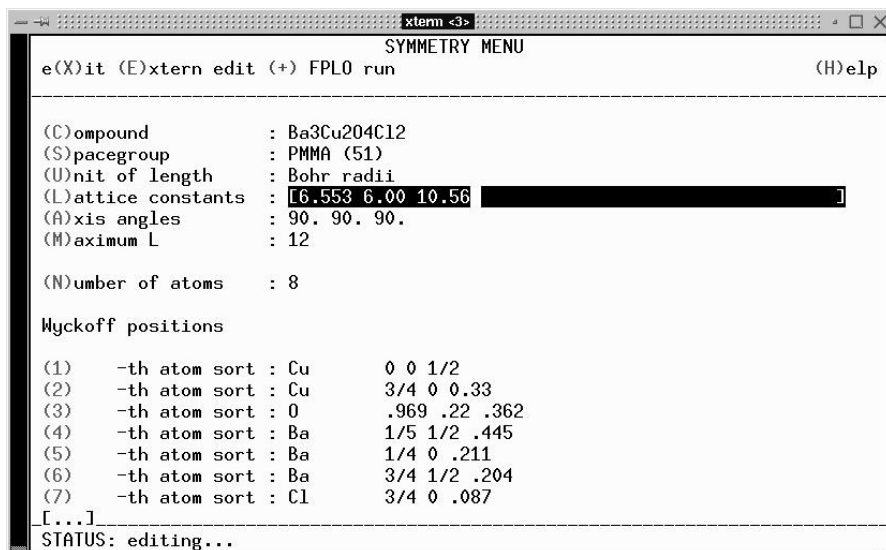[3]The release number 2 refers to the year 2002.

Portability

What is needed for installing and using FPLO®-2, is a UNIX-derived operating system with ANSI-conform C compiler and f90 compiler. We have tested the portability for the following platforms:

operating system	compiler
Linux	ifc
Linux	pgf90
IRIX	vendor f90
True64	vendor f90
AIX	vendor f90
HP-UX	vendor f90

Note, that we cannot guaranty the function on other platforms. In particular, other than the mentioned f90 compilers may yield reduced performance or do not suite at all. In any case, it is highly recommendable to use the most recent compiler release.

User interface

The user interface comprises not only the necessary tools to set up and modify the input files for running the code, but also several tools for presentation and processing the output data. Figure 10 shows a screen-shot of the specifically designed input-editor. It runs interactively with the main FPLO code, is operated by hot-keys and largely error-resistant. The example shown is $Ba_3Cu_2O_4Cl_2$, an anti-ferromagnetic compound out of the large family of the copper-oxides containing 22 atoms per elementary cell. More complicated elementary cells may consist of more than one hundred atoms.

Figure 10: Screen-shot of the FPLO input tool.

Understanding the geometrical structure of a compound is an important condition for understanding its bonding and, in succession, all other chemical and physical properties. For this aim, a related presentation tool is utterly useful. Figure 4 has been produced with this tool.

Other tools are available for the presentation of Fermi surfaces and band structures on symmetry lines, including weighted ('fat') bands, and for the supervision of the iteration process.

Benchmarks

There are two quantities that chiefly determine the computing time and the memory allocation: the number of atoms in the elementary cell, and the number of k-points.[4] We present two example benchmarks here, the dependence of computing time per iteration cycle and memory allocation on the number of k-points, and the memory allocation in dependence of the complexity of the elementary cell. More extended benchmark tests will be presented at the FPLO homepage
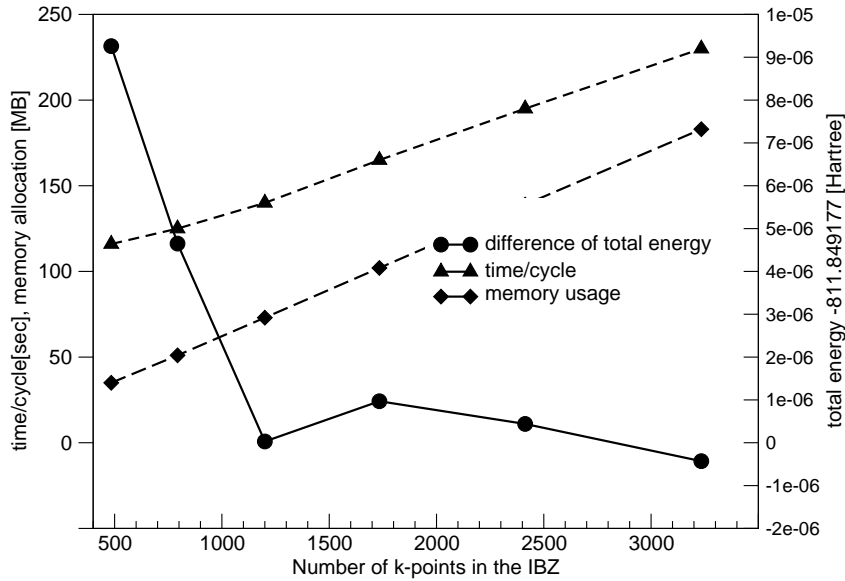

Figure 11: Example benchmark: ScB_2 with 3 atoms per unit cell, self consistent calculation with different numbers of k-points. Left axis: computing time per iteration cycle and memory allocation; right axis: total energy. The calculation was done on Origin3800, running IRIX6.5.

Figure 11 shows the dependence of computing time and memory allocation on the number of k-points in the irreducible part of the Brillouin zone for the example compound ScB_2 with 3 atoms per unit cell. As expected, both the computing time per iteration cycle and the memory allocation scale linearly with the number of k-points. There is a significant constant contribution to the computing time, i.e., choosing a large number of k-points does not significantly slow

---

[4]In a strict sense, the number of k-points is of course determined by the accuracy requirements and cannot be chosen arbitrarily.

Table 1: Example benchmark: Memory allocation (on Origin3800, IRIX6.5) in dependence of the structure and number of k-points.

Compound	atoms/u.c.	k-points in IBZ	Memory [MB]
Al	1	72	6
Fe	1	72	9
ScB_2	3	191	63
$SrCoO_3$ cubic	5	35	27
$SrCoO_3$ orthorhombic	5	1331	555

down the calculation for small unit cells (up to about 10 atoms). Another important feature is that the total energy of the self consistent calculation is stable (for sufficiently large number of k-points) within 1 μHartree.

Some examples of the memory needed for different structures are compiled in Table 1. In cases were large numbers of k-points in the irreducible part of the Brillouin zone (IBZ) are needed the memory allocation is considerable already for unit cells of moderate size. We plan to implement a version with reduced memory demand in the forthcoming release.

Workshop "Hands-on-FPLO"

From March 3 to 7, 2002, IFW Dresden hosted the workshop "Hands-on-FPLO" that was supported by the ESF, STRUC-ψ_k. Purpose of the tutorial workshop was to provide an introduction into the concept, the code, and the handling of the FPLO package including the ability to cope with simple problems that may arise when using the code.

The workshop programme consisted of lectures held by the code developers and by experienced users of the code primarily in the morning hours, and exercises in the afternoon. While the first exercise was focussed on "getting started" (fcc-aluminum: how to create the input file, meaning and handling of the output), all participants were able to work on systems of their individual choice during the second and third day of the workshop. The number of participants (30 trainees from 9 different countries and 11 lecturers) was almost twice the originally planned number, demonstrating the need of fast and accurate DFT code. Twelve X-terminals, each connected to a separate dual node of our LINUX cluster, were available to the participants. In this way, the group size could be kept moderately small and (almost) individual work was possible.

As the main result of the workshop, all participants are able to handle the code for routine calculations. The participants further started calculations on systems of their choice. In cases were difficulties with the code handling encountered, they could be solved together with the tutors. Licenses to use the code for academic purposes were issued to the home departments of all participants (15 in total). The second workshop "Hands-on-FPLO" is scheduled for March,

2003.

Summary and Outlook

We finally summarize the features of the recently developed full-potential local-orbital minimum-basis (FPLO) scheme in brief.

- FPLO uses a locally finite lattice sum for the representation of the full potential by a partitioning of unity. This enables a treatment of the multi-center integrals both efficient and accurate.

- The algebraic dimension of the problem is reduced by a fast and exact elimination of the core states.

- FPLO uses a variable local orbital basis which is readjusted to the potential at each iteration step of self-consistency.

- During the iterations of self-consistency, the basis orbitals are simultaneously optimized by individual parameter variation to minimize the total energy.

- Given a density functional, FPLO has a thoroughly tested numerical accuracy of better than 2 mHartree per atom for the absolute value of the total energy.

- Up to about N=100 atoms per unit cell, FPLO performs approximately as $N^{1.5}$. It is extremely efficient with a large number of $\mathbf{k}$-points, an important issue in applications to metals.

- There exist a fully 4-component relativistic version, a scalar relativistic version, and a flexible CPA implementation for substitutional alloys. Rotationally invariant LSDA+U is implemented as well.

As an outlook, we intend to release FPLO®-3, comprising the present release and the fully relativistic code, in 2003.

Acknowledgment

References

[1] K. Koepernik and H. Eschrig, Phys. Rev. B **59**, 1743 (1999).

[2] H. Eschrig and I. Bergert, phys. stat. sol. (b) **90**, 621 (1978).

[3] H. Eschrig, *Optimized LCAO Method and the Electronic Structure of Extended Systems* (Springer-Verlag, Berlin, 1989).

[4] A. Ernst, PhD thesis, TU Dresden, 1997.

[5] R. Richter, H. Eschrig, and B. Velicky, J. Phys. F **17**, 351 (1987).

[6] K. Koepernik, B. Velicky, R. Hayn, and H. Eschrig, Phys. Rev. B **55**, 5717 (1997).

[7] K. Koepernik, B. Velicky, R. Hayn, and H. Eschrig, Phys. Rev. B **58**, 6944 (1998).

[8] M. Richter, Beiträge zur Theorie relativistischer Effekte in der elektronischen Struktur metallischer Systeme, PhD thesis, TU Dresden, 1988.

[9] M. Richter and H. Eschrig, Solid State Commun. **72**, 263 (1989).

[10] I. Opahle, PhD thesis, TU Dresden, 2001.

[11] R. Feder, F. Rosicky, and B. Ackermann, Z. Phys. B **52**, 31 (1983).

[12] D. D. Koelling and B. N. Harmon, J. Phys. C **10**, 3107 (1977).

[13] J. Boettger, Phys. Rev. B **57**, 8743 (1998).

[14] J. Ruvalds and L. Falicov, Phys. Rev. **172**, 508 (1968).

[15] J. P. Perdew and Y. Wang, Phys. Rev. B **45**, 13244 (1992).

[16] P. Söderlind, L. Nordström, L. Yongming, and B. Johansson, Phys. Rev. B **42**, 4544 (1990).

[17] P. Söderlind, O. Erikson, B. Johansson, and J. M. Wills, Phys. Rev. B **50**, 7291 (1994).

[18] M. D. Jones, J. C. Boettger, R. C. Albers, and D. J. Singh, Phys. Rev. B **61**, 4644 (2000).

[19] J. Kuneš *et al.*, Phys. Rev. B **64**, 153102 (2001).

[20] O. K. Andersen, Phys. Rev. B **12**, 3060 (1975).

[21] L. Nordström *et al.*, Phys. Rev. B **63**, 035103 (2000).